Supporting information

Highly Exfoliated $Ti_3C_2T_x$ MXene Nanosheets Atomically Doped with Cu for Efficient Electrochemical CO_2 Reduction: An Experimental and Theoretical Study

Kamel Eid[a*], Qingqing Lu[b], Safwat Abdel-Azeim[c], Ahmed Soliman [a], Aboubakr M. Abdullah[d], Ahmed M. Abdelgwad[a], Roy P. Forbes[e], Kenneth I. Ozoemena[e], Rajender S. Varma[f]*, and Mohamed F. Shibl[g]

[a] Gas Processing Center (GPC), College of Engineering, Qatar University, Doha 2713, Qatar

[b] Engineering &Technology Center of Electrochemistry, School of Chemistry and Chemical Engineering, Qilu University of Technology (Shandong Academy of Sciences), Jinan 250353, China

[c] Center for Integrative Petroleum Research (CIPR), College of Petroleum Engineering and Geosciences, King Fahd University of Petroleum and Minerals (KFUPM), Dhahran 31261, Saudi Arabia

[d] Center for advanced materials, Qatar University, Doha 2713, Qatar

[e] Molecular Sciences Institute, School of Chemistry, University of the Witwatersrand, Private Bag 3, P O Wits, Johannesburg 2050, South Africa

[f] Regional Centre of Advanced Technologies and Materials, Czech Advanced Technology and Research Institute, Palacky University, Slechtitelu 27, 783 71 Olomouc, Czech Republic.

[g] Department of Chemistry and Earth Sciences, College of Arts and Sciences, Qatar University, P.O. Box 2713, Doha, Qatar

*Corresponding authors: kamel.eid@qu.edu.qa and varma.rajender@epa.gov

Table of contents

Electrochemical CO_2 reduction reaction (CO_2RR)

The electrochemical cyclic voltammogram (C.V.s), linear sweep voltammogram (LSV), impedance spectroscopy (EIS), and constant potential electrolysis (CPE) were measured using a Gamry electrochemical analyzer (reference 3000, Gamry Co., USA). The electrochemical three-electrode cell consisted of a Pt wire (counter centrode), Ag/AgCl (reference electrode), and glassy carbon ((G.C.), working electrode). All the measurements were carried out in an aqueous solution of 0.1 M $NaHCO_3$ at room temperature. After measurements, the liquid products were collected and analyzed using the nuclear magnetic resonance (NMR) 600 MHz (NMR, JEOL). ^{1}H-NMR measurements were carried out at 400.2 MHz in the presence of D_2O solution (35 µL) of 10mM dimethyl sulfoxide (DMSO) and 50 mM phenol as the internal standards. Standard formic acid (0, 10, 30, and 50mM) solutions mixed with the D_2O solution (35 µL) containing 10 mM DMSO and 50mM phenol were prepared to quantify the amount of formic acid in the electrolytes. Then, the relative area of the HCOO- signal concerning phenol was plotted versus HCOO- concentration to obtain a calibration curve. For ^{13}C-NMR deuterated chloroform ($CDCl_3$) with Tetramethylsilane (Me4Si) were used as an internal standard.

Fabrication of the working electrode

Vitreous glassy carbon electrode (⌀15 mm x 1 mm) was polished using (1 µm) and then (0.3 µm) alumina slurry (Buehler). After each polishing step, the substrate was rinsed in double deionized water (DDI-H_2O) for 30 sec under ultrasonic treatment at room temperature. The catalyst ink was prepared by mixing 2 mg of each catalyst is added into 1 mL DDI-H_2O water and 0.2 mL ethanol (absolute grade, Sigma Aldrich Chemicals) and 40 uL of Nafion solution

(5 Wt.% mixture, Sigma Aldrich) under sonication in an ice bath for 5 min). The inks were deposited volumetrically onto the polished glassy carbon with a 0.5 mg/cm^{-2} loading amount and then left to dry in an oven at 50 ^{o}C.

Density functional theory simulation details

The Vienna ab initio simulation package (VASP) has been used for all DFT simulations, along with the projector augmented wave pseudopotentials (PAW) using periodic boundary conditions. The Brillouin zone has been sampled with a 1×1×1 Monkhorst-pack gamma-based mesh, and Gaussian smearing of 0.02 eV was employed for the electronic levels occupation. The electron interaction energy of exchange-correlation has been described using the Perdew-Burke-Ernzerhof (PBE) functional within the generalized gradient approximation (GGA). The considered conversion limit of the electronic energies has been within the limit of 10^{-7} eV and a 520 eV cutoff. A 0.02 eV/Å force criteria have been used for all geometries. The Van der Waals (vdW) dispersion corrections are adopted using Grimme's D3 scheme. The initial structure of Ti_3C_2 has been built from its hexagonal MAX phase Ti_3AlC_2 by removing the Al layer.[1] The resulting Ti_3C_2 structure is composed of three layers of Ti and two layers of carbon. A supercell of 441 $Ti_3C_2T_x$ is created, where T_x is the surface terminations (x = O, F, and a mixture of O, F, and O.H.). The EDX results confirmed Ti, C, O, F, and Cu with atomic ratios of about 50.09, 31.79, 10.2, 6.7, and 1.04 %, respectively. Two-dimensional four structures are built to study the effect of the different surface functionalization on the CO_2 reduction reaction (CO_2RR) profile. Four systems have been built; a fully terminated with O, F, and a mixture of O, F, and O.H.; in the latter, we have replaced one Ti by Cu to mimic the experimental atomic ratios of the Cu-doped MXene. This mode of Cu-doping has been inspired by Pt-doping studies of $Ti_3C_2T_x$ reported by Zhao et al.[2]. They confirmed that the Pt atoms are confined in Ti-vacancies created during the exfoliation process. The CO_2RR reaction profile on Ti_3C_2Tx has been studied using the computational hydrogen electrode approach pioneered by Nørskov et al.[3]

We have simulated the CO_2RR reaction using the following mechanism:

$CO_2(g) + * \rightarrow *CO_2$ Equation 2

$*CO_2 + H^+ + e^- \rightarrow *COOH$ Equation 3

$*COOH + H^+ + e^- \rightarrow *HCOOH$ Equation 4

$*HCOOH \rightarrow * + HCOOH$ Equation 5

The free energies of all the species at zero electrode potential have been calculated as follows: $G(U) = \Delta E + \Delta ZPE - T\Delta S$, where ΔE represents the change in enthalpy, which is considered as the DFT total energies, ΔZPE depicts the change in zero-point energy, T is the absolute temperature, and ΔS is the change in entropy. The * represents the catalyst. Therefore, at the zero-electrode potential, the free energy change of the four steps can be summarized as the following:

$\Delta G_1 = G_{*CO2} - G_* - G_{CO2(g)}$ Equation 6

$\Delta G_2 = G_{*COOH} - G_{*CO2} - 0.5\ G_{H2(g)}$ Equation 7

$\Delta G_3 = G_{*HCOOH} - G_{*COOH} - 0.5\ G_{H2(g)}$ Equation 8

$\Delta G_4 = G_* + G_{HCOOH} - G_{*HCOOH}$ Equation 9

Entropy and zero-point energy for H_2 (g) are taken from Nørskov et al.[3]. The entropy and zero-point corrections for the adsorbed species are calculated using the finite difference method as implemented in VASP, analyzed using VASPKIT.[4]

Table S1 The comparison between the preparation method, shape, and composition of our newly designed $Cu/Ti_3C_2T_x$ and previous reported MXene-based catalyst for CO_2RR.

Catalysts	**Preparation method**	**Type of reaction**	**Ref.**
Cu atomic doped $Ti_3C_2T_x$	$Ti_3C_2T_x$ was formed by HF etching method and then doped with Cu by simple impregnation with Cu salt at room temperature under stirring. The mass loading of Cu dopant was (1.04 Wt. %).		This work
Ti_3C_2 quantum dots (QDs) impeded in 1D Cu_2O wires	Cu_2O wires obtained by anodic oxidation of Cu mesh, while Ti_3C_2 QDs formed by a hydrothermal method and passivated by polyethylenimine (PEI). Ti_3C_2 QDs were assembled over Cu_2O wires passivated with poly(sodium4-styrenesulfonate) followed by annealing at 200 °C for 1 h. The mass ratio of Ti_3C_2Tx was 0.2-1 mg/mL.	Photocatalytic	[5]
2D nanosheets Ti_3C_2/2D nanosheets $Bi_2\ WO_6$	Ti_3C_2 formed by H.F. etching then used as support for the growth of $Bi_2\ WO_6$ by the hydrothermal treatment at 120 °C for 24 h. The mass ratios of Ti_3C_2/Bi_2WO_6 were as 0.5/99.5, 1/99, 2/98, and 5/95%.	Photocatalytic	[6]
Commercial spherical TiO_2 P25 nanoparticles decorated 2D Ti_3C_2-OH nanosheets	Ti_3C_2-OH prepared by the HF etching followed by alkylation and mixing physically in water with P25 for 12 h. The mass ratios of Ti_3C_2-OH were from 1-10 wt %.	Photocatalytic	[7]
TiO_2 nanoparticles (NPs) distributed over 2DTi_3C_2 nanosheets	Ti_3C_2 formed by HF method then annealed with TiO_2 through calcination method at 350-650 ^oC. The loading amount of TiO_2 was 15-99.9 %.	Photocatalytic	[8]

$CsPbBr_3$ nanocubes distributed over 2D Ti_3C_2 nanosheets	Ti_3C_2 by HCl-HF etching and was used as support for the growth of $CsPbBr_3$ by a hot-injection method. The loading amount of Ti_3C_2 10, 20, 30, 50 mg.	Photocatalytic	9
3D hierarchical structure Co-Co layered double hydroxide/$Ti_3C_2T_x$ nanosheets	Ti_3C_2-OH prepared by the HF etching and used as a support for the growth of Co-Co by solvothermal method. The loading amounts of Co were 38.78-49.6.	Photocatalytic	10
2D g-C_3N_4 nanosheets impeded within 2D Ti_3C_2 nanosheets	Ti_3C_2 was prepared by the H.F. etching then annealed with urea for growth of 2D g-C_3N_4. The loading amounts of Ti_3C_2 were 5-15 wt %.	Photocatalytic	11
Cube-like CeO_2 over Ti_3C_2 nanosheets	Ti_3C_2 nanosheets were used as support for the growth of CeO_2 cubes by the hydrothermal at 180 °C for 24 h. The mass ratios of Ti_3C_2 were 3-7 wt %.	Photocatalytic	12
2D $Ti_3C_2T_x$ nanosheets with 2D g-C_3N_4 nanosheets	Ti_3C_2-OH formed by the H.F. etching followed by alkalization then mixed in an aqueous solution for 12 h with g-C_3N_4 obtained by annealing at 550 ^{o}C. The mass loadings of Ti_3C_2-OH were 1, 5, 10, 15 wt%.	Photocatalytic	13
2DTiO_2/2D C_3N_4/0D Ti_3C_2	2D mesoporous TiO_2 nanosheets synthesized via hydrothermal induced solvent-confined monomicelle self-assembly were used as a support for the growth of 2D C_3N_4 nanosheets by annealing of urea, then TiO_2/C_3N_4 was mixed via electrostatic interactions with 0D Ti_3C_2 QDs that obtained by HF etching and hydrothermal treatment at 100 ^{o}C for 6 h.	Photocatalytic	14
2Dg-C_3N_4/2D bentonite/2D $Ti_3C_2T_x$	2D g-C_3N_4 nanosheets formed by hydrothermal method and 2D $Ti_3C_2T_x$ nanosheets by H.F. etching, and both were mixed with bentonite by stirring for 6vh and sonication for 1 h.	Photo- catalytic	15
ZnO-Fe-$Ti_3C_2T_x$	ZnO prepared by hydrothermal at 453 K for 12 h then calcination in at 673 K for 2 h and ZnO-Fe by the hydrothermal and calcination at 673 K for 2 h then mixed with HF obtained $Ti_3C_2T_x$ by hydrothermal at 453 K for 12 then calcination at 673 K for 2 h. The mass ratio of ZnO-Fe was 32.27 wt %.	Electro-catalytic	16
2D MoC_2T_x nanosheets 2D Ti_2CT_x nanosheets	Ti_2CT_x formed by HF etching or KF-HCl, while MoC_2T_x Formed by HF etching.	Electro-catalytic	17
Metal (Pd, Pt, and Au) N.P.s/ 2D g-C_3N_4 nanosheets/2D Ti_3C_2 nanosheets	Ti_2CT_x formed by HF etching and was annealed at 500 ^{o}C for 2 h with thiourea to be decorated with gC_3N_4. The mass contents of Ti_3C_2/g-C_3N_4 were 50/1 (denoted as $TCCN_1$), 20/1 (denoted as $TCCN_1$) and 10 /1 (denoted as $TCCN_3$). Then metal (Pd, Pt, and Au) N.P.s were deposited by electrodeposition over2D	Photo-Electro-catalytic	18

	g C_3N_4/decorated 2D Ti_3C_2.		
Co_3O_4 nanorods anchored on 2D $Ti_3C_2T_x$-NH_3 nanosheets	$Ti_3C_2T_x$-NH_3 formed by HF and annealing under NH_3 at 600 °C, then was used as support for the growth of Co_3O_4 by chemical impregnation and annealing at 350 °C for 2 h. The mass loading of Co was 9.8 wt %.	Thermal CO_2 hydrogenation	19
Pd/N-TiO_2/$Ti_3C_2T_x$/FTO	N-TiO_2/$Ti_3C_2T_x$ was prepared by the H.F. etching followed by hydrothermal oxidation and salinization under refluxing for 6 h to and then deposited over FTO to form N-TiO_2/$Ti_3C_2T_x$/TFO. Pd was deposited over N-TiO_2/$Ti_3C_2T_x$/TFO by pulse electrodeposition technique. The loading amount of Pd is 0.83 wt %.	Artificial photosynthesis	20

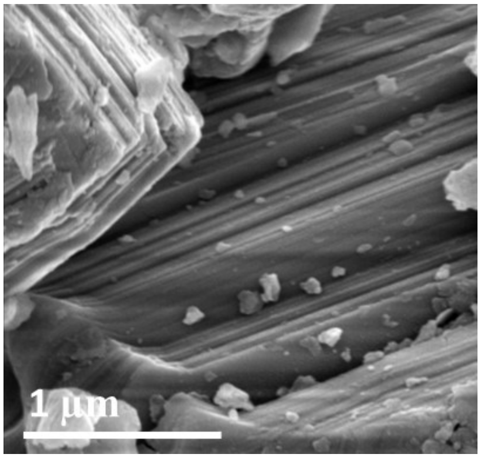

Figure S1 SEM image of Ti_3AlC_2

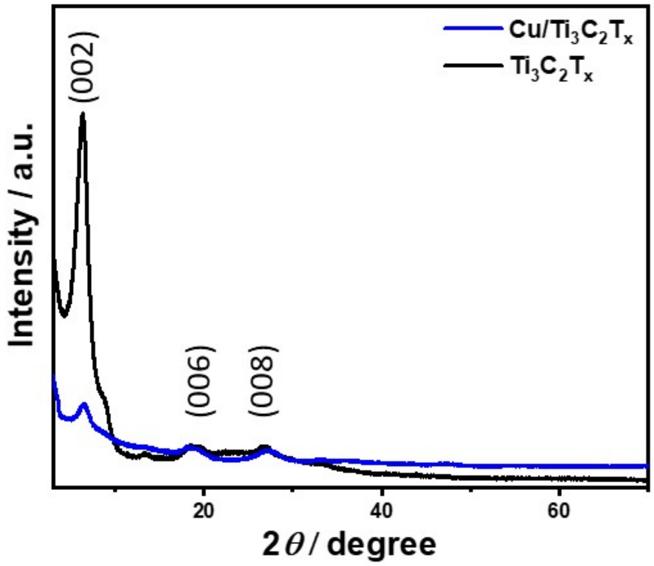

Figure S2 XRD of Cu/$Ti_3C_2T_x$ and $Ti_3C_2T_x$.

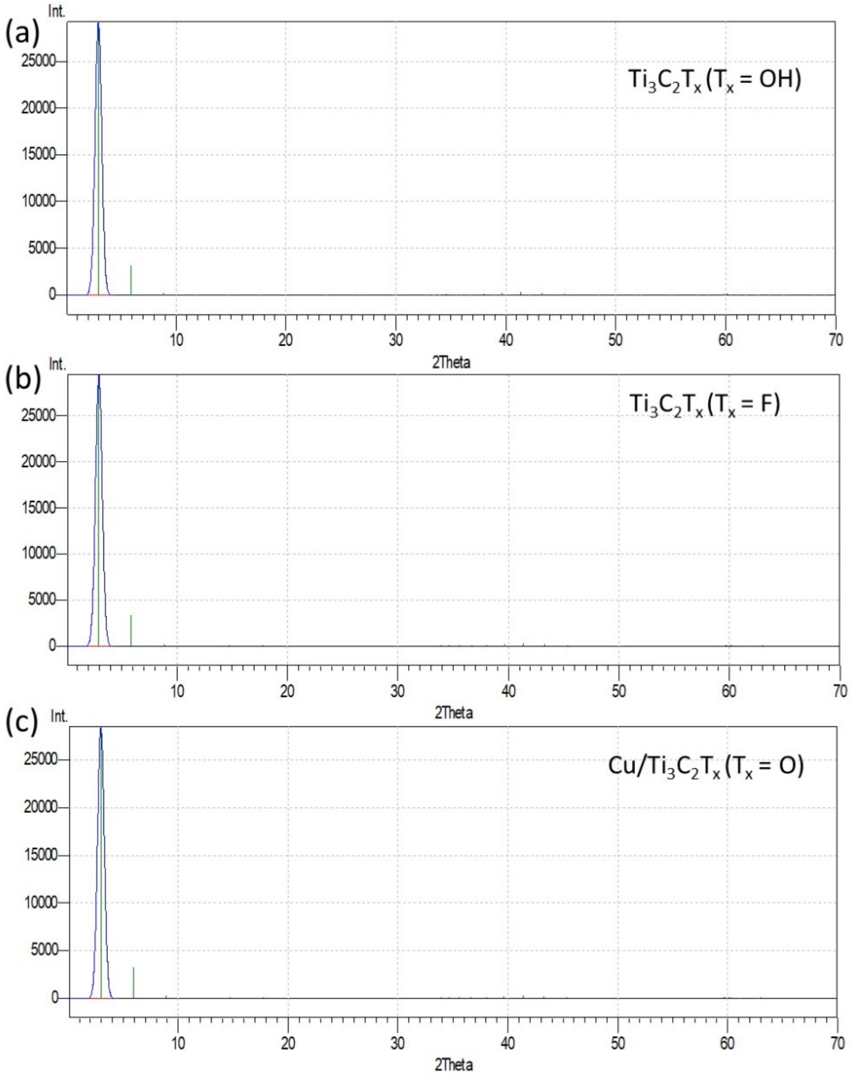

Figure S3 Powder X-ray diffraction retrieve of $Ti_3C_2T_x$ as a function of Tx (Tx= F, O, and OH).

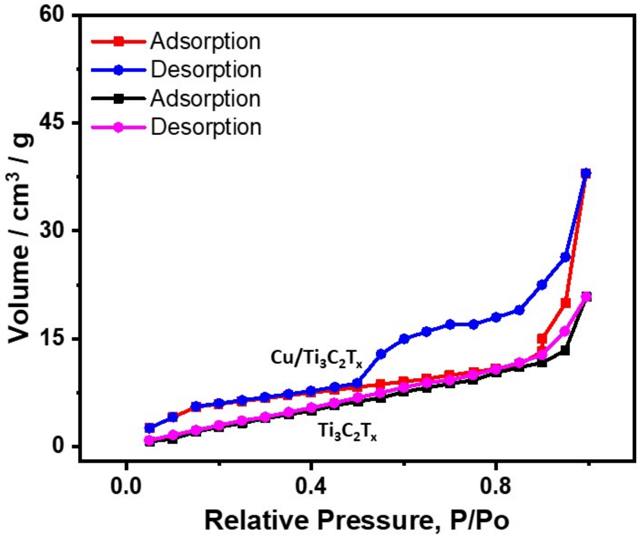

Figure S4 Nitrogen adsorption/desorption isotherms of Cu/$Ti_3C_2T_x$ and $Ti_3C_2T_x$.

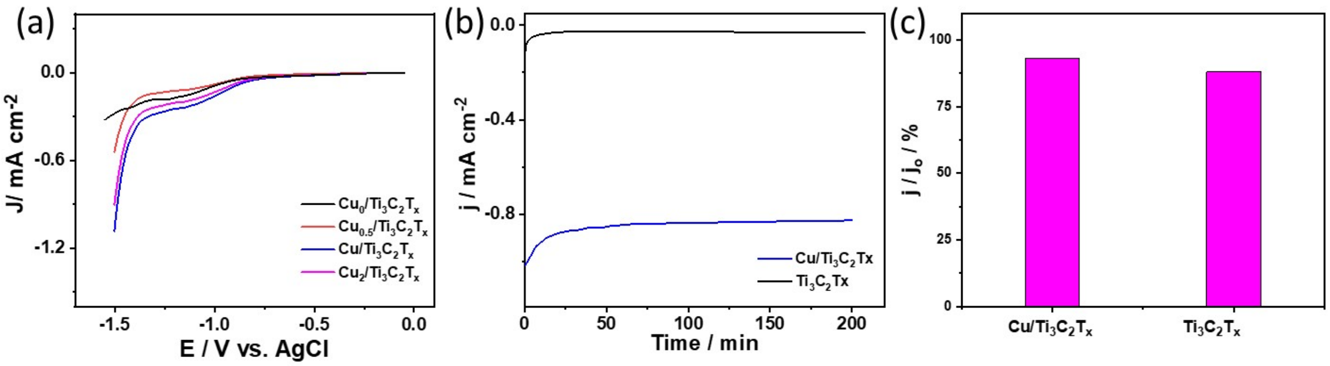

Figure S5 (a) LSV measured in a CO_2-saturated 0.1 M $NaHCO_3$ solution at room temperature on $Cu_0/Ti_3C_2T_x$, $Cu_{0.5}/Ti_3C_2T_x$, Cu/$Ti_3C_2T_x$, and $Cu_2/Ti_3C_2T_x$. (b) The constant potential electrolysis (CPE) tests measured in a CO_2-saturated 0.1 M $NaHCO_3$ solution at room temperature at -1.5 V and (c) the calculated *j*/*j*$_o$ percent after 200 min for Cu/$Ti_3C_2T_x$ relative to $Ti_3C_2T_x$.

Table S2. The CO_2RR performance and their related conditions over MXenes reported elsewhere compared with our newly developed Cu/$Ti_3C_2T_x$ MXene. * Refers to the Faradic efficiency.

Catalyst	Photocurrent density/Current density	Type of reaction/Conditions	Product	Faradic efficiency, Yield/Rate	Ref.
Cu/ $Ti_3C_2T_x$	-1.08 mA cm^{-2} at -1.5 $V_{Ag/AgCl}$	Electro- catalytic 25 ^oC Electrolyte 0.1 M $NaHCO_3$	HCOOH -CH_3OH	*58.1%	This work
- Ti_3C_2 sheets/ Cu_2O NWs/Cu - Ti_3C_2 QDs/ Cu_2O NWs/Cu	- 4.29 mA cm^{-2} at 0 V_{RHE} - 5.84 mA cm^{-2} at 0V_{RHE}	Photo-catalytic AM 1.5, 300 W Xe lamp Electrolyte Na2SO4 (0.5 m, pH = 5.8 with potassium phosphate 0.1 m)	-CH_3OH	- 153.38 ppm cm^{-2} after 6 hours - 70.25 ppm cm^{-2} after 6 h	5
Ti_3C_2/Bi_2 WO_6	- 3.25 µA cm^{-2} at 0V_{RHE}	Photo-catalytic 300 W Xe lamp Electrolyte 0.5 mol/L potassium sulfate solution (pH = 7)	- CH_3OH -CH_4	- 2.64 µmol g^{-1} after 6 h - 10.68 µmol g^{-1} after 6 h	6
Ti_3C_2-OH/Commercial TiO_2	- 8.0 µA cm^{-2} at 0$V_{Ag/AgCl}$	Photo- catalytic 300 W Xe lamp Electrolyte 0.5 M 0.5 M Na2SO4	- C.O. - CH_4	- 70.44 µmol g^{-1} after 6 h - 99.66 µmol g^{-1} after 6 h	7
Ti_3C_2/TiO_2	- 6.0 µA cm^{-2} at 1.2 $V_{Ag/AgCl}$	Photo- catalytic 300 W Xe lamp Electrolyte 0.5 M Na2SO4	- CH_4	- 26.4 µmol g^{-1} after 6 h	8
$CsPbBr_3$/MXene	0.05 nA	Photo-catalytic 300 W Xe lamp (>420 nm) Electrolyte Ethyl acetate	- C.O. - CH_4	- 24.75 µmol g^{-1} after 6 h - 11.44 µmol g^{-1} after 6 h	9
Co-Co LDH/$Ti_3C_2T_x$	- N/a	Photocatalytic 5 W LED lamp (400-1000 nm) Acetonitrile/H2O/triethanolamine	- CO	12.5 mmol h^{-1} g^{-1}	10
Ti_3C_2/g-C_3N_4	- N/a	Photo- catalytic 300 W Xenon lamp (λ ≥ 420 nm)	- C.O. - CH_4	- 5.19 µmol h^{-1} g^{-1} - 0.044 µmol h^{-1} g^{-1}	11

		Electrolyte g $NaHCO_3$ (1.26) powders+ 2M H_2SO_4			
CeO_2/Ti_3C_2	4.11 µA cm^{-2} at -0.57 $V_{Ag/AgCl}$	Photo- catalytic 350 W Xe lamp. Electrolyte NaHCO3 (0.084 g)+2M HCl	- CO	39.67 µmol m^{-2} h^{-1}	12
$Ti_3C_2T_x$/ g-C_3N_4	1.99 nA cm^{-2}	Photo- catalytic 50 W Xenon lamp Electrolyte 0.2 M Na2SO4	- C.O. - CH_4	- 11.21 µmol g^{-1} - 0.203 µmol g^{-1}	13
2D/2D/0D $TiO_2/C_3N_4/Ti_3C_2$	-0.42 µA cm^{-2} at -0.2 V	Photo- catalytic Xenon lamp Electrolyte $NaHCO_3$ (0.084) + 2M H_2SO_4	- C.O. - CH_4	- 4.39 µmol h^{-1} g^{-1} - 1.20 µmol h^{-1} g^{-1}	14
2D/2D/2D O-C_3N_4/Bt/$Ti_3C_2T_x$	- N/a	Photo- catalytic	- CO - CH_4	- 326 µmol h^{-1} g^{-1} - 230 µmol h^{-1} g^{-1}	15
ZnO-Fe-$Ti_3C_2T_x$	18 mA/cm^2 at -1 $V_{Ag/AgCl}$	Electro-catalytic 35 W HID lamp Electrolyte 0.5 NaOH	NA	- N/A	16
2D MoC_2T_x 2D Ti_2CT_x (KF-HCL etchant) 2D Ti_2CT_x (H.F. etchant)	-1.1 mA cm^{-2} at -1.5 V_{SHE} -2.5 mA cm^{-2} at -1.55 V_{SHE} −0.51 mA cm^{-2} at -1.5 V_{SHE}	Electro- catalytic Electrolyte acetonitrile, water, and 3-butyl-1-methyl-1H-imidazol-3-iumtetra-fluoroborate (BMIMBF4)	- HCOOH - CO -HCOOH -HCOOH	*38 % *1.1% *20.7% *56.1 %	17
Pd/$TCCN_3$ Pt/$TCCN_3$ Au/$TCCN_3$ $TCCN_3$	-1.2 mA at 1.4V -1.5 V vs. Ag/AgCl 1.25 mA 1.16 mA 1.1 mA	Photo-Electro –catalytic 300 W xenon lamp Electrolyte 0.1 M KHCO3 aqueous	HCOO- CH_3OH Hydrocarbon	37 µmol h^{-1} cm^{-2} 14 µmol h^{-1} cm^{-2} 50.2 µmol h^{-1} cm^{-2}	18
Co_3O_4 nanorods/2D $Ti_3C_2T_x$-NH_3 nanosheets	−0.75 mA cm^{-2} -0.29 V vs. SHE	Thermal catalytic	HCCOH	53368 µmol h^{-1} g^{-1}	19

Pd/N-TiO_2/$Ti_3C_2T_x$/FTO	-10 mA cm^{-2} -1.4 V vs. SCE	Photo-Electro –catalytic 300 W Xe lamp (200 mW/cm^2) Electrolyte 0.1M $KHCO_3$	HCOOH CH_3OH, CH_3CH_2OH	45 µmol h^{-1} cm^{-2} 28 µmol h^{-1} cm^{-2} 5 µmol h^{-1} cm^{-2}	20

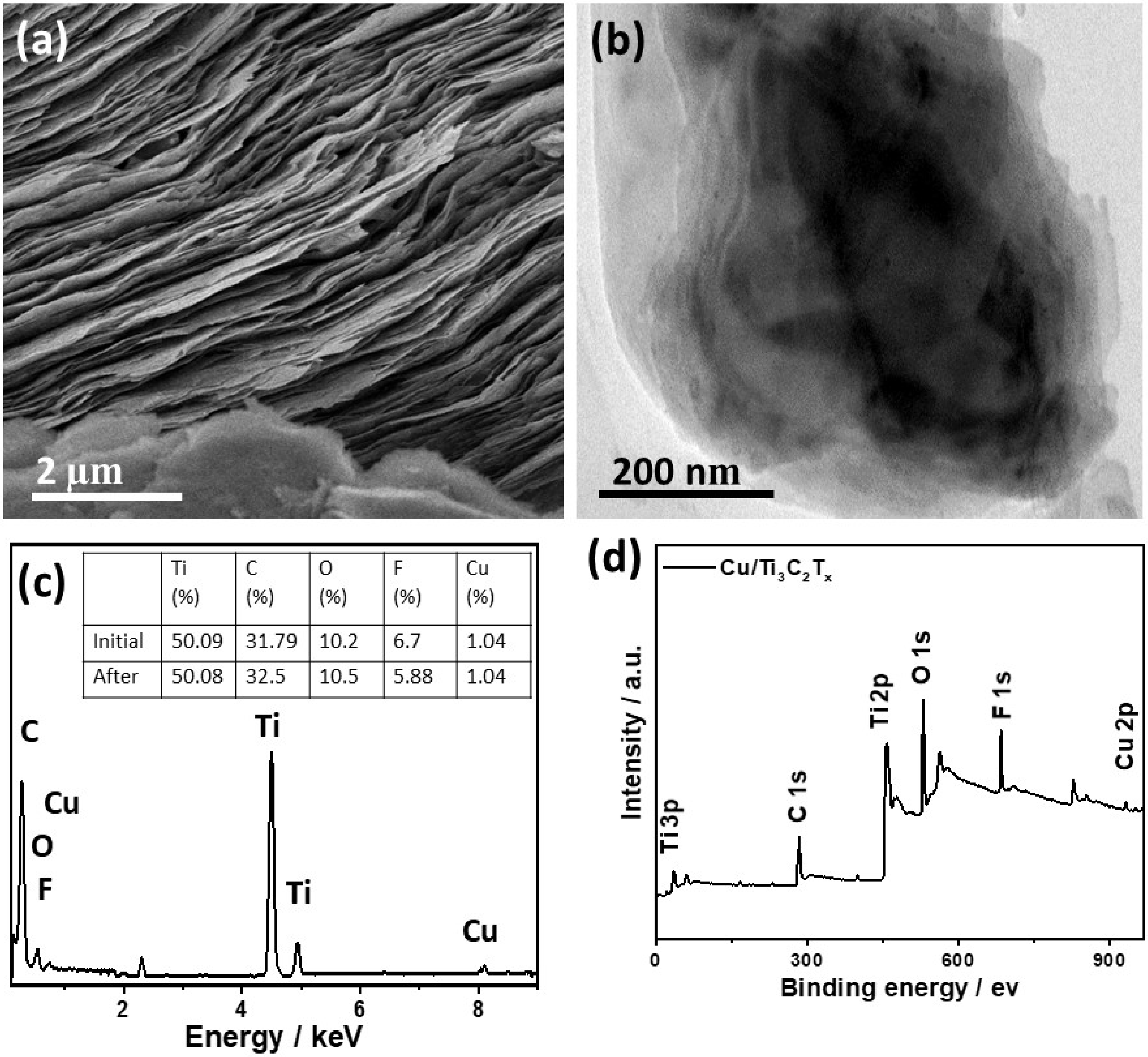

	Ti (%)	C (%)	O (%)	F (%)	Cu (%)
Initial	50.09	31.79	10.2	6.7	1.04
After	50.08	32.5	10.5	5.88	1.04

Figure S6 (a) SEM image, (b) TEM image, (c) EDX analysis, and (d) XPS survey of Cu/$Ti_3C_2T_x$ after CPE durability test. The table in (b) shows the estimated composition before and after stability tests determined using the EDX.

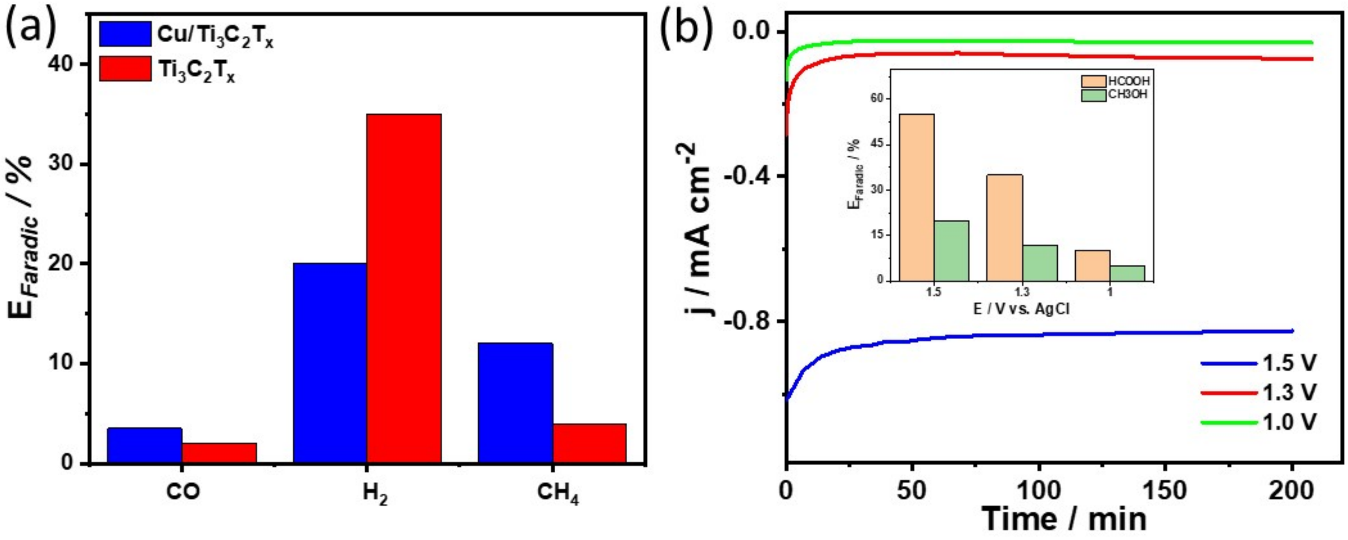

Figure S7 (a) E_{Fradic} of minor CO_2RR products obtained on $Cu/Ti_3C_2T_x$ and $Ti_3C_2T_x$ at -1.5V.The gas products were analyzed using gas chromatography (GC) (Wasson-ECE Instrumentation, Colorado USA) using the same protocol in Ref.[21] (b) CPE testes measured on $Cu/Ti_3C_2T_x$ under differ poetical and its related $E_{Fradaic}$ of HCOOH and CH_3OH at various potential.

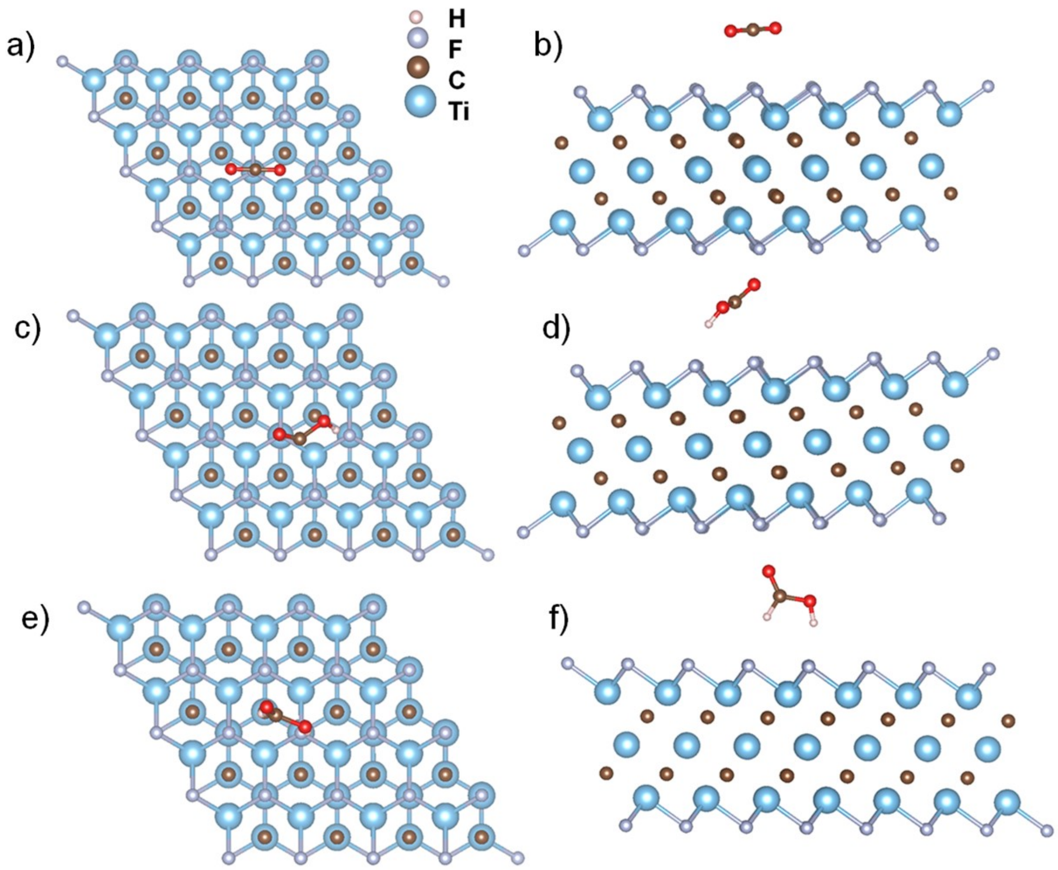

Figure S8 Top and side view of $^*CO_2$ (a,b),$^*COOH$ (c,d), $^*HCOOH$ (e,f) intermediates optimized on $Ti_3C_2T_x$ (T_x=F)

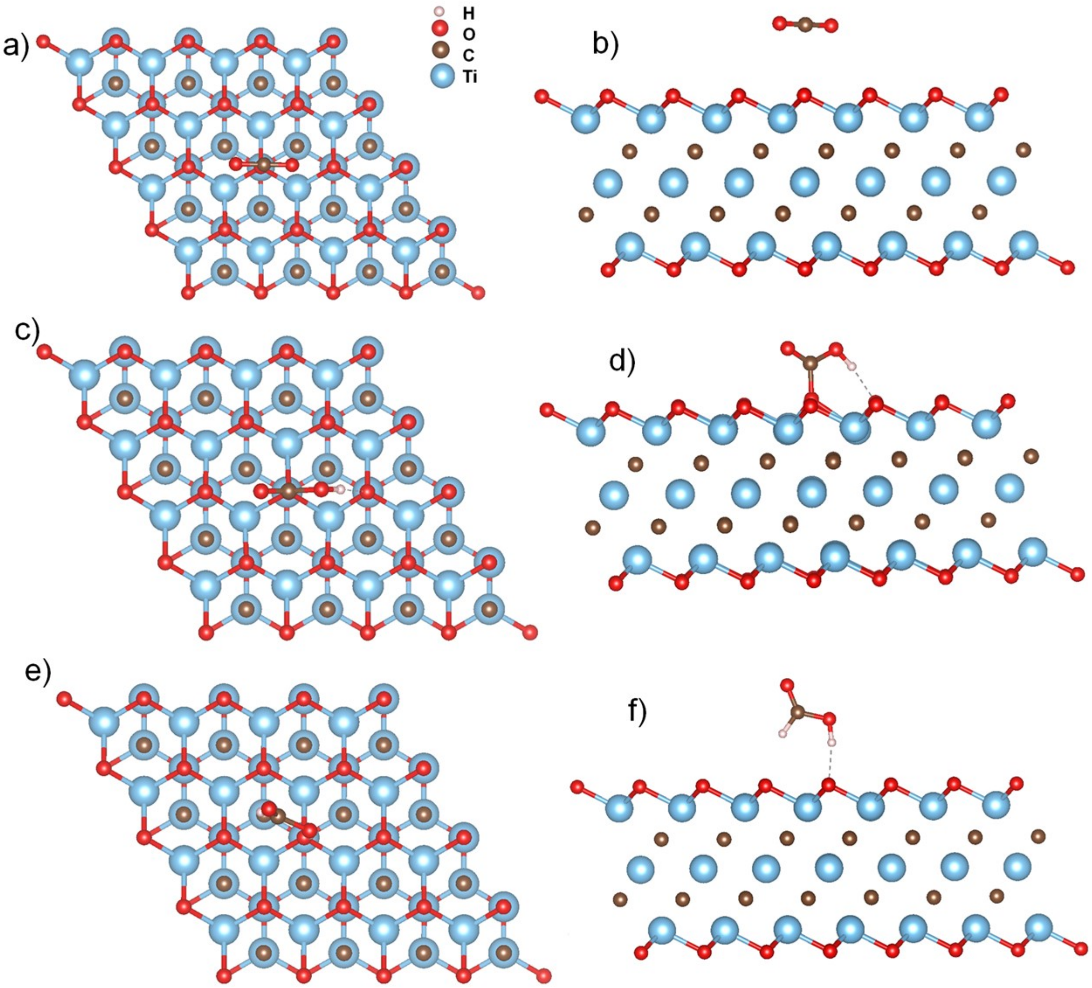

Figure S9 Top and side view of $*CO_2$ (a,b),$*COOH$ (c,d), $*HCOOH$ (e,f) intermediates optimized on $Ti_3C_2T_x$ (T_x=O)

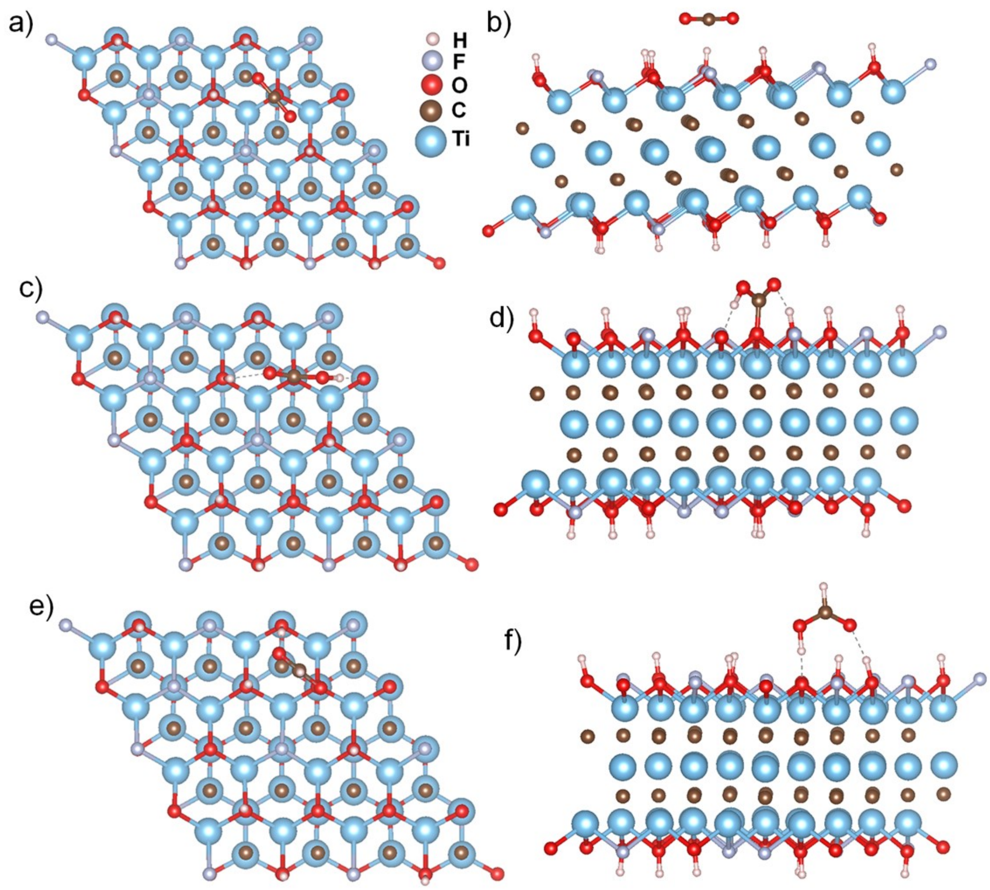

Figure S10 Top and side view of $*CO_2$ (a,b),*COOH (c,d), *HCOOH (e,f) intermediates optimized on $Ti_3C_2T_x$ (T_x=F, O, and OH)

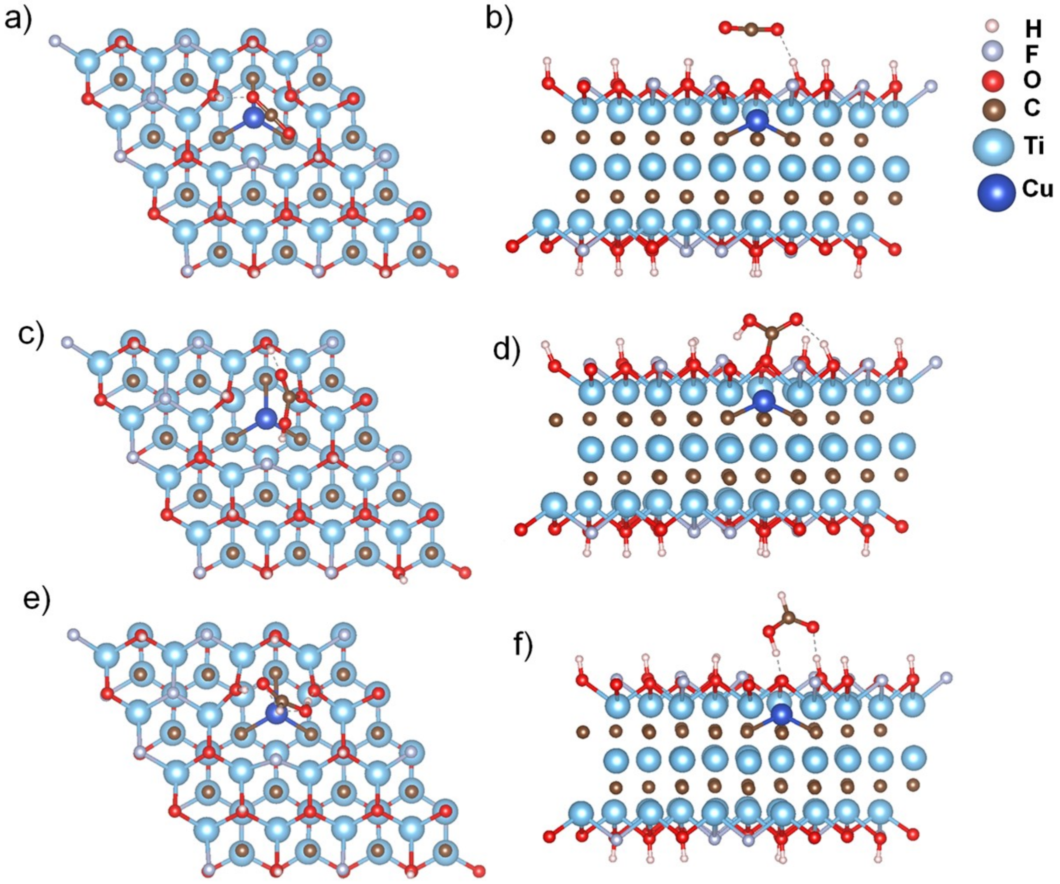

Figure S11 Top and side view of $^*CO_2$ (a,b),$^*COOH$ (c,d), $^*HCOOH$ (e,f) intermediates optimized on Cu/$Ti_3C_2T_x$ (T_x=F, O, and OH)

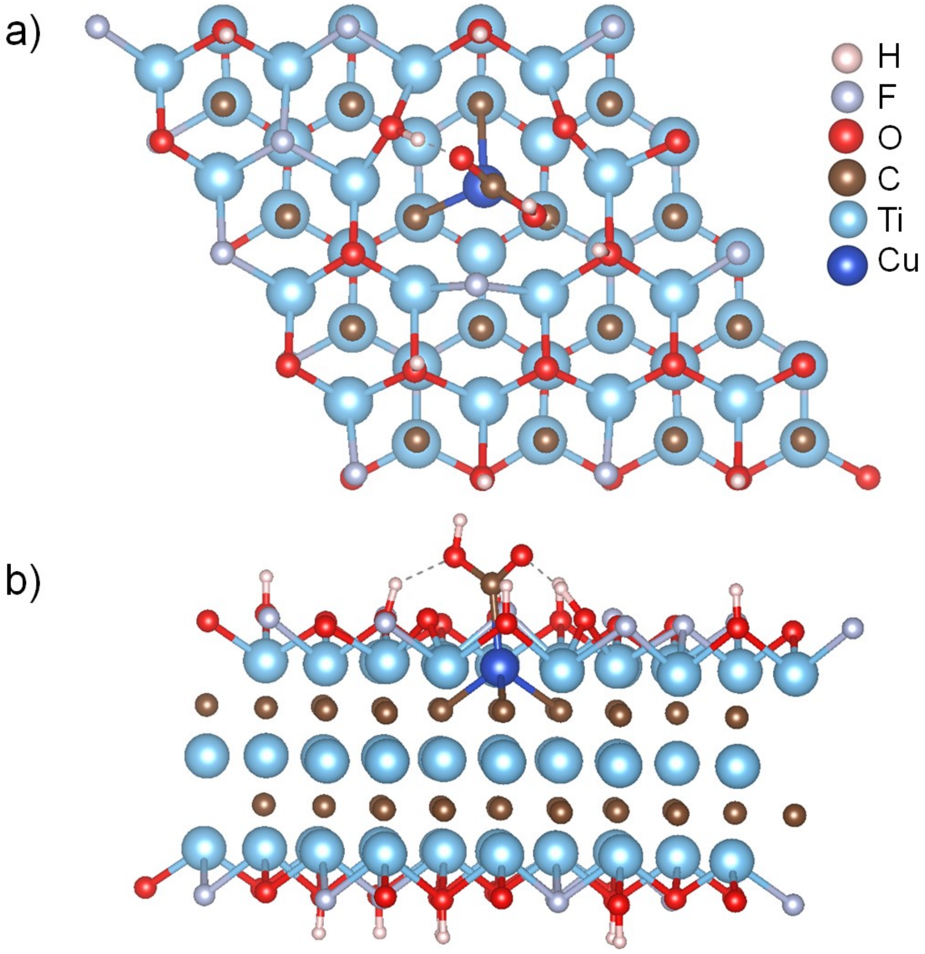

Figure S11 Top (a) and side view (b) of *COOH intermediate optimized on Cu/$Ti_3C_2T_x$ (T_x=F, O, and OH)

References

1. N. V. Tzenov and M. W. Barsoum, *Journal of the American Ceramic Society*, 2000, **83**, 825-832.
2. D. Zhao, Z. Chen, W. Yang, S. Liu, X. Zhang, Y. Yu, W.-C. Cheong, L. Zheng, F. Ren and G. Ying, *Journal of the American Chemical Society*, 2019, **141**, 4086-4093.
3. J. K. Nørskov, J. Rossmeisl, A. Logadottir, L. Lindqvist, J. R. Kitchin, T. Bligaard and H. Jonsson, *The Journal of Physical Chemistry B*, 2004, **108**, 17886-17892.
4. V. Wang, N. Xu, J.-C. Liu, G. Tang and W.-T. Geng, *Computer Physics Communications*, 2021, 108033.
5. Z. Zeng, Y. Yan, J. Chen, P. Zan, Q. Tian and P. Chen, *Advanced Functional Materials*, 2019, **29**, 1806500.
6. S. Cao, B. Shen, T. Tong, J. Fu and J. Yu, *Advanced Functional Materials*, 2018, **28**, 1800136.
7. M. Ye, X. Wang, E. Liu, J. Ye and D. Wang, *ChemSusChem*, 2018, **11**, 1606-1611.
8. J. Low, L. Zhang, T. Tong, B. Shen and J. Yu, *Journal of Catalysis*, 2018, **361**, 255-266.
9. A. Pan, X. Ma, S. Huang, Y. Wu, M. Jia, Y. Shi, Y. Liu, P. Wangyang, L. He and Y. Liu, *The journal of physical chemistry letters*, 2019, **10**, 6590-6597.

10. W. Chen, B. Han, Y. Xie, S. Liang, H. Deng and Z. Lin, *Chemical Engineering Journal*, 2020, **391**, 123519.
11. C. Yang, Q. Tan, Q. Li, J. Zhou, J. Fan, B. Li, J. Sun and K. Lv, *Applied Catalysis B: Environmental*, 2020, **268**, 118738.
12. J. Shen, J. Shen, W. Zhang, X. Yu, H. Tang, M. Zhang and Q. Liu, *Ceramics International*, 2019, **45**, 24146-24153.
13. Q. Tang, Z. Sun, S. Deng, H. Wang and Z. Wu, *Journal of Colloid and Interface Science*, 2020, **564**, 406-417.
14. F. He, B. Zhu, B. Cheng, J. Yu, W. Ho and W. Macyk, *Applied Catalysis B: Environmental*, 2020, **272**, 119006.
15. M. Tahir and B. Tahir, *Chemical Engineering Journal*, 2020, **400**, 125868.
16. K. Kannan, M. H. Sliem, A. M. Abdullah, K. K. Sadasivuni and B. Kumar, *Catalysts*, 2020, **10**, 549.
17. A. D. Handoko, H. Chen, Y. Lum, Q. Zhang, B. Anasori and Z. W. Seh, *Iscience*, 2020, **23**, 101181.
18. Y. Xu, S. Wang, J. Yang, B. Han, R. Nie, J. Wang, Y. Dong, X. Yu, J. Wang and H. Jing, *Journal of Materials Chemistry A*, 2018, **6**, 15213-15220.
19. J. Ma, Q. Jiang, Y. Zhou, W. Chu, S. Perathoner, C. Jiang, K. H. Wu, G. Centi and Y. Liu, *Small*, 2021, 2007509.
20. Y. Xu, S. Wang, J. Yang, B. Han, R. Nie, J. Wang, J. Wang and H. Jing, *Nano Energy*, 2018, **51**, 442-450.
21. A. D. Handoko, H. Chen, Y. Lum, Q. Zhang, B. Anasori and Z. W. Seh, *Iscience*, 2020, 101181.